Eur. Phys. J. Special Topics **223**, 1859–1867 (2014)

DOI: 10.1140/epjst/e2014-02231-x

THE EUROPEAN PHYSICAL JOURNAL SPECIAL TOPICS

Regular Article

Electrohydrodynamic controlled assembly and fracturing of thin colloidal particle films confined at drop interfaces

Z. Rozynek[1,2,a], P. Dommersnes[3], A. Mikkelsen[1], L. Michels[1], and J.O. Fossum[1,b]

[1] Department of Physics, Norwegian University of Science and Technology, Hoegskoleringen 5, 7491 Trondheim, Norway
[2] Institute of Physical Chemistry, Polish Academy of Sciences, Kasprzaka 44/52, 01-224 Warsaw, Poland
[3] Matière et Systèmes Complexes, Université Paris 7 Diderot, 10, rue Alice Domon et Léonie Duquet, 75205 Paris, France

Received 30 June 2014 / Received in final form 21 July 2014
Published online 22 September 2014

Abstract. Particles can adsorb strongly at liquid interfaces due to capillary forces, which in practice can confine the particles to the interface. Here we investigate the electrohydrodynamic flow driven packing and deformation of colloidal particle layers confined at the surface of liquid drops. The electrohydrodynamic flow has a stagnation point at the drop equator, leading to assembly of particles in a ribbon shaped film. The flow is entirely controlled by the electric field, and we demonstrate that AC fields can be used to induce hydrodynamic "shaking" of the colloidal particle film. We find that the mechanical properties of the film is highly dependent on the particles: monodisperse polystyrene beads form packed granular monolayers which "liquefies" upon shaking, whereas clay mineral particles form cohesive films that fracture upon shaking. The results are expected to be relevant for understanding the mechanics and rheology of particle stabilized emulsions.

1 Introduction

There is an increasing interest in studying the self-assembly of colloids by using electric fields [1]. A charged particle movement in electric fields may ensure controlled assembly where the electric force acts directly on the particles. For example, the direct control given by electric field effects can be used for manipulating the self-assembly in electrophoretic displays [2], electronic ink [3], to study lane formation [4], or concentrating particles by dielectrophoretic motion [5]. In contrast, it has been demonstrated that electric field indirectly can order suspended colloidal aggregates due to induced fluid flows [6]. Such electrohydrodynamic (EDH) flows can induce convective deposition of colloidal particles [6–9], and this is at the heart of the present

[a] e-mail: zrozynek@ichf.edu.pl
[b] e-mail: jon.fossum@ntnu.no

work. Convective driven assembly of colloidal particles, can also be induced by for example evaporation, such as in the much-studied "coffee ring" effect [10–12], and can be employed for creating ordered particle monolayers or crystals [13,14]. Different types of deposit patterns can also be achieved by for example balancing evaporation and surface tension driven flows [15].

In an emulsion drop formed and surrounded by leaky-dielectric liquids, free charge accumulation can result in a Maxwell electric stress that induces liquid circulation flows inside and outside the drop [16,17], known as EHD flows. Recently we demonstrated that these flows, in similar manner to the convective evaporating flows present in the "coffee ring" effect, can be used to assemble colloidal ribbons on drop surfaces [7]. In our method [7] colloidal particles are carried by EHD flows rather than by electric forces acting on them directly.

In general, the packing of particles is dependent on factors like deposition rates, temperature or application of external forces. The deposition rate can be tuned in various ways, for example in the coffee ring effect it can be achieved by controlling of a drop's evaporation rate. When the evaporation rate is low, particles have sufficient time to find optimal arrangements by Brownian motion, resulting in a higher ordered packing [18]. Packing density can also be controlled by repetitive application of external force. An example of such behavior can be found in a granular media, where thermal cycles can be used to systematically increase the packing density of grains. During the cycles, differences in thermal expansion of the container and grains can induce small rearrangements that allow the grains to settle into denser arrangements [19]. Packing of particles is also important in Pickering emulsions, for which the stability depends on the defects sizes in the colloidal shell covering each drop [20]. Thus more optimal arrangement and packing of particles within a shell may improve Pickering emulsions stability.

In the present study we demonstrate how electric cycles (by employing AC E-fields) aid jammed surface particles to explore configuration space, resulting in more dense packing and the formation of highly ordered particle structures. The experiments reported here were designed to highlight the importance of the forced particle deposition dynamics on the static packing arrangements. Our investigations show how the particle packing density relates to the deformation of the drop and the EHD flow inside and outside the drop, both enabling the surface confined particles to relocate and settle.

2 Experimental set-up and materials

The experimental set up and its components are presented in Fig. 1. The sample cell, used for the experiments, was made of glass ($10 \times 10 \times 30$ mm) where two of the walls were coated with conductive ITO (Indium Tin Oxide), constituting electrodes. The cell was filled with castor oil (Sigma-Aldrich 83912, specific density of $0.961\,\mathrm{gcm}^{-3}$ at 25 °C, electric conductivity $45\,\mathrm{pSm}^{-1}$, relative permittivity 4.7 and viscosity <1000 cSt). Silicone oil drops containing polyethylene (PE) particles were immersed in the castor oil using a regular mechanical pipette (as shown in the right panel of Fig. 1). Two silicone oils (Dow Corning 200/10 cSt and 200/100 cSt, electric conductivity approximately 3–5 pSm^{-1}, relative permittivity 2.1) with different densities (0.960 and $0.965\,\mathrm{gcm}^{-3}$ at 25 °C) were mixed to match the castor oil density and thus minimizing the buoyance force on the drop. The colloidal PE particles used for the experiments were purchased from Cospheric LLC and had diameters ranging from 27–32 μm (specific density of $1\,\mathrm{gcm}^{-3}$). In the preparation stage, silicone oil and colloidal particles were measured by weight and stirred together, followed by ultrasonic bath treatment to minimize aggregation. All videos were recorded using

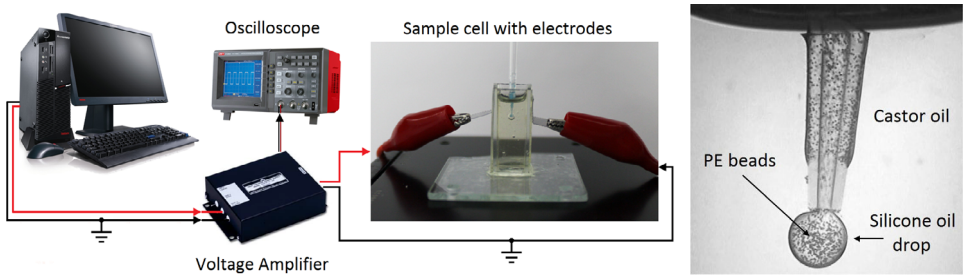

Fig. 1. The experimental set-up consists of a PC for adjusting applied voltage and frequency, a voltage amplifier, an oscilloscope for monitoring signal shape and amplitude, and a sample cell placed on a mechanical stage. The cell is made of glass ($10 \times 10 \times 30$ mm) where two of the walls are coated with ITO layer to which conductive tape is attached. A drop containing colloidal particles is formed using a regular mechanical pipette (right panel).

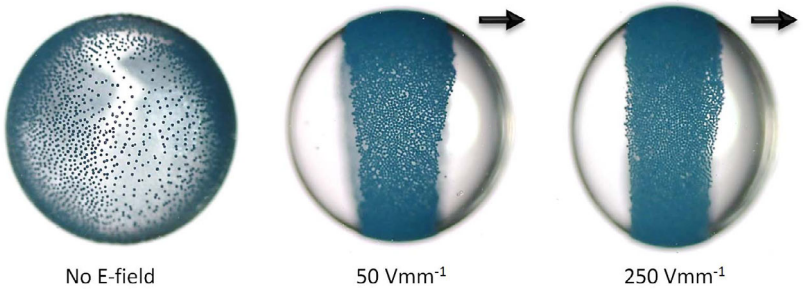

Fig. 2. PE particles trapped at the drop surface are guided towards the drop's electrical equator and assembled into a 'ribbon-like' structure. The particle packing density increases with the applied E-field strength. The black arrows indicate the direction of the E-field lines.

a digital camera mounted on a stereoscope, and the observation view was always perpendicular to the electric field (E-field), which in the figures is in the horizontal direction.

3 Results

3.1 Packing of particles in DC electric fields

With the aforementioned preparations and set-up in place, one can study electric-field-guided assembly from non-conductive colloidal particles that are already located on the oil-oil interface. The particles can be brought to the drop surface by any suitable method of choice, such as particle sedimentation, used in our experiments. We took advantage of the density mismatch between colloidal particles and silicone oil. It takes a few minutes for the particles to sediment and reach the drop interface. They adsorb to the oil-oil interface due to strong capillary binding [21], so the movement and reorganization of particles during the experiment is confined to the drop surface. After all the particles have adsorbed, we randomly distribute them on the drop surface (see Fig. 2a) by means of mechanical action. Subsequently, an electric field is applied across the sample cell, inducing EHD liquid flows inside and outside the drop [16]. The EHD flow has a stagnation point at the drop equator and guides the colloidal particles there forming a monolayered ribbon structure [7]. The packing density of

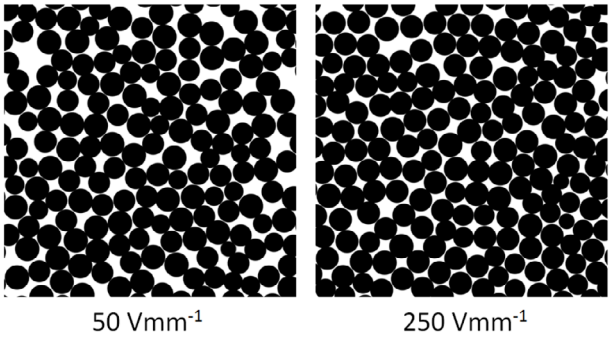

Fig. 3. Processed images of the particle ribbon on the drop surface. The PE particles assembled at a low E-field strength, $\mathrm{E} = 50\,\mathrm{Vmm}^{-1}$, are clearly more loosely packed compared to the structure formed at $\mathrm{E} = 250\,\mathrm{Vmm}^{-1}$.

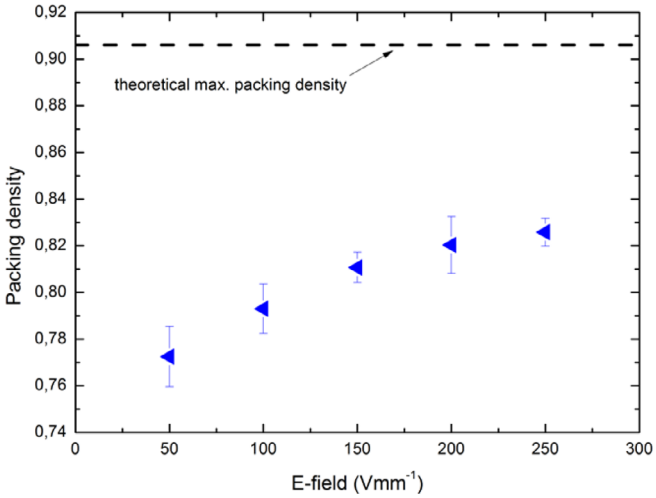

Fig. 4. Particle packing density as a function of the E-field strength. The dashed line represents the upper theoretical limit [22] for monodisperse close packed spheres forming a 2-D monolayer.

the assembled ribbon depends on the applied electric field strength (see Fig. 2b and Fig. 2c).

As shown in Fig. 2, PE particles assembled at $E = 50\,\mathrm{Vmm}^{-1}$ are noticeably more loosely packed compared to the structure formed at $E = 250\,\mathrm{Vmm}^{-1}$. To quantify the degree of particle confinement, raw images were computer processed (as shown in Fig. 3) and the packing densities were calculated to be $\sim$0.77 and $\sim$0.82 for the experiments performed at E-field strengths 50 and $250\,\mathrm{Vmm}^{-1}$, respectively. The colloidal particles used here were slightly polydisperse and the surface is slightly curved. A typical PE colloidal size distribution is presented in Fig. S1[1]. Theoretically, for monodisperse spheres forming a 2-D monolayer the maximum packing fraction is $\sim$0.91 [22].

Figure 4 shows how the packing density relates to the E-field strength. After the particle ribbon is formed at $50\,\mathrm{Vmm}^{-1}$, the E-field strength is increased by $50\,\mathrm{Vmm}^{-1}$ and maintained ($<$1 min) until a new meta-stable configuration is reached, i.e. the

[1] Supplementary material will be available electronically on the web.

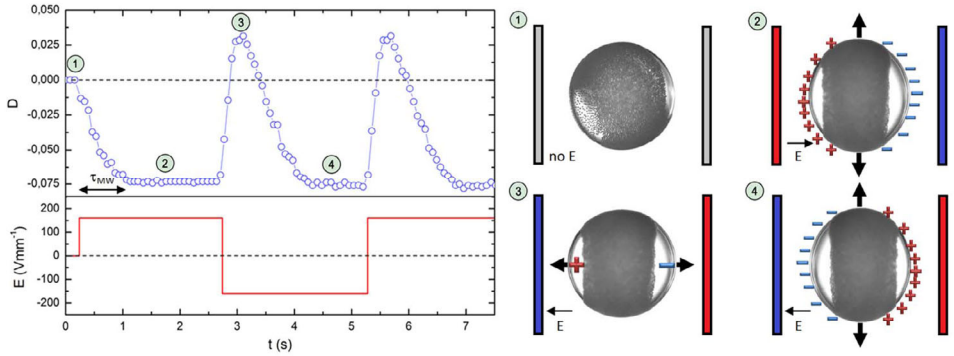

Fig. 5. Shape (Oblate ↔ Prolate) transition of a silicone oil drop. The drop deformation is plotted as function of time. No E-field is applied and $D = 0$ (1). After the E-field is turned on, the drop deforms into an oblate shape and $D < 0$ (2). Right after the E-field polarity is inverted, the drop becomes prolate ($D > 0$) for a short time (3). As the charges re-build on the drop surface, the drop deforms back into an oblate shape again (4).

PE particles had enough time to re-arrange within "the same initial" ribbon. The maximum E-field strength applied in this experiment was $250\,\mathrm{Vmm}^{-1}$. Applying stronger E-fields, increases liquid circulations, which makes the ribbon unstable, and the ribbon breaks into several rotating domains [7].

Dipolar interactions between the PE particles used here are negligibly small [7] (see also Fig. S2[2]) compared to the hydrodynamic forces responsible for carrying the particles to a drop surface. Also thermal energies can be neglected for the particles sizes used here. The packing density is determined by: (i) the EHD flow velocity inside and outside the drop working on the particles in the *direction towards* the electric equator, and (ii) the electro-deformation of the drop (the ribbon's circumference increases with increasing E-field due to the drop's oblate deformation [16]) enabling the particles to re-locate in the *direction along* the ribbon. After the particles re-arrange the system is in a meta-stable configuration. When the E-field is turned off, the colloidal particles relax and the particle assembly unjams.

3.2 Packing of particles in low frequency AC square electric fields

We anticipate that a successive two-way movement of colloidal particles in directions both along and across the ribbon can influence the packing fraction due to the re-arrangement of colloidal particles. This may lead to a formation of denser particle configurations.

We validate this assumption by utilizing the shape (Oblate ↔ Prolate) transition (oblate deformation: $D < 0$ and prolate deformation: $D > 0$) of a drop occurring when the applied E-field direction changes. Such a transition is presented in Fig. 5, where the deformation (D) is plotted as function of both time and E-field direction. The drop deformation is here defined as $D = \frac{d_{\parallel} - d_{\perp}}{d_{\parallel} + d_{\perp}}$, where $d_{\parallel}$ and $d_{\perp}$ are the drop's diameters in the direction parallel and perpendicular to the electric field lines. At $t = 0\,\mathrm{s}$, the drop is spherical and $D = 0$. After the E-field is applied, the drop obtains an oblate shape ($D < 0$) due to the EHD liquid flows induced by the charge build-up on the drop surface (for more details see [16,23]). In our castor oil-silicone oil system, the Maxwell-Wagner charge build-up time [23] of a drop is $\tau_{\mathrm{MW}} \sim 1.1\,\mathrm{s}$. The τ_{MW}

[2] Supplementary material will be available electronically on the web.

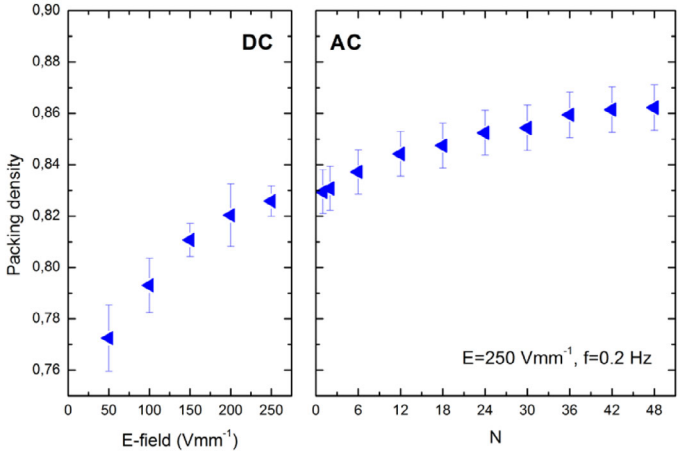

Fig. 6. The effect of applying low frequency AC E-field (right panel). Deforming the drop at frequency $f = 0.2\,\mathrm{Hz}$ induces successive vertical and horizontal vibrations of colloidal particles. The packing density increases after each oscillation period. The final measured packing density ($N = 48$) increased by around 5% compared to the packing density obtained before the AC E-field was applied ($N = 0$).

is defined as $\tau_{\mathrm{MW}} = \frac{2\epsilon+\tilde{\epsilon}}{2\sigma+\tilde{\sigma}}\epsilon_0$, where ϵ is electric conductivity and σ is the dielectric constant of the surrounding liquid (castor oil). The tilde denotes the values for the drop liquid (silicone oil). When the E-field polarity changes, the drop rapidly deforms into a prolate shape ($D > 0$). While the E-field polarity changes instantaneously, it takes finite time for charges to re-distribute on the drop surface (of the order of τ_{MW}). As this is occurring, there is a short moment when the EHD flow is significantly reduced and the drop dipole is aligned in the same direction as E-field, which can explain the prolate shape deformation. As the charges are building up on the oil-oil interfaces and the Taylor EHD flows are induced again, the drop is pushed into an oblate shape. The shape (Oblate $\leftrightarrow$ Prolate) transition of a drop will consequently aid to move colloidal particles in directions both towards/outwards the ribbon and upwards/downwards along the ribbon.

Figure 6 shows the effect of applying a low frequency AC E-field to the same drop as presented in the previous section, where the influence of the DC E-fields (blue triangles on the left panel) was studied. The highest packing density obtained using DC E-fields was ∼0.82, observed at $E = 250\,\mathrm{Vmm}^{-1}$. At this point the experiment is continued and the drop is still exposed to an E-field of $250\,\mathrm{Vmm}^{-1}$. However, now we introduce the successive two-way movement of colloidal particles in directions both along and across the ribbon by deforming the drop at frequency $f = 0.2\,\mathrm{Hz}$ (the frequency has to be chosen such that the charges have enough time to build-up on the drop surface, i.e. cycle period is longer than τ_{MW}). After each oscillation period, the packing density increases and its value starts to reach a plateau after around 40 periods. After and due to the induced oscillations of the colloidal particles, the packing density increased by around 5%.

It should be brought to attention that if the frequency is chosen adequately (the E-field polarity changes before the ribbon breaks into small rotating domains), much stronger AC E-fields can be used (up to 400 Vmm^{-1}) when compared to the ribbon stable maximum values of the DC E-field (up to 250 Vmm^{-1}). By using stronger E-fields it is possible to move particles with higher amplitude (motion in horizontal direction) and further away from the ribbon.

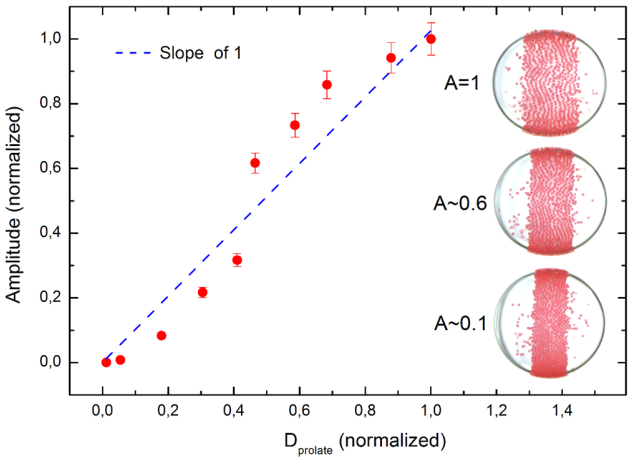

Fig. 7. Amplitude of particle movement in direction toward/outward the ribbon as function of prolate deformation.

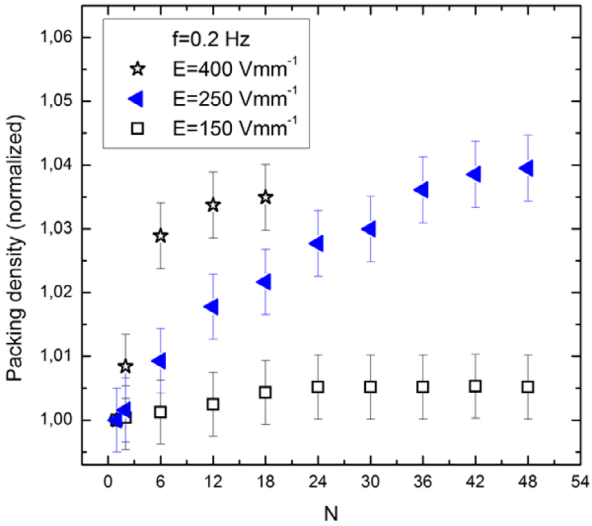

Fig. 8. The amplitude strength of particle horizontal and vertical motions (that depends on a drop deformation, hence the E-field strength) affects the packing density dynamics. The packing density was normalized to its value at N = 1 for each E-field strength.

Figure 7 shows normalized amplitude (A) values of particle movement in direction toward/outward the ribbon as function of normalized prolate deformation (D_{prolate}). The normalized amplitude is calculated as the ratio between the longest ribbon width (when drop is prolately shaped) at a certain E-field strength and the shortest ribbon width (when drop is oblately shaped). The obtained ratio values were then subtracted by 1 and normalized to the value at the strongest E-field, similar to the deformation normalization.

The amplitude strength of particle horizontal and vertical motions, which depends on a drop deformation and hence the strength of E-field, affects the packing density dynamics, as shown in Fig. 8. Due to the fast drop motion towards one of the electrodes, it was only possible to study the particle packing at $E = 400\,\text{Vmm}^{-1}$ for a short time. That explains why only five data points are plotted (open stars) for this E-field strength.

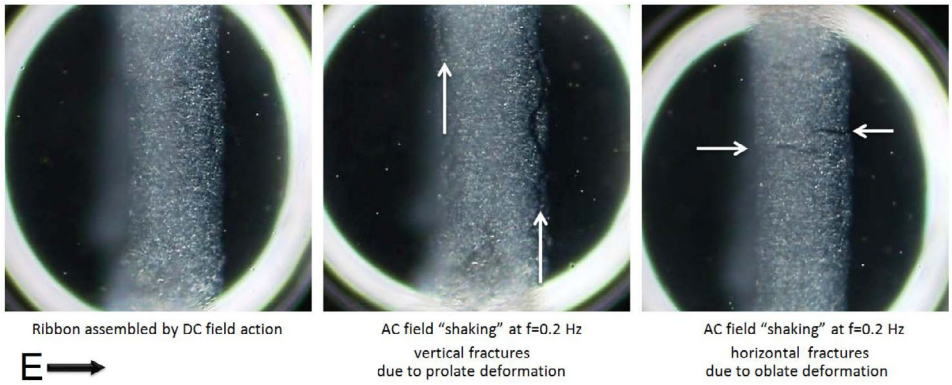

Fig. 9. Ribbon structure assembled from laponite clay minerals by a DC E-field of $250\,\mathrm{Vmm}^{-1}$ (left panel). Application of an AC E-field deforms the drop. Vertical fracturing is observed during prolate deformation (middle panel), and horizontal fracturing appears during oblate deformation (right panel). AC E-field strength was $300\,\mathrm{Vmm}^{-1}$ and frequency $f = 0.2\,\mathrm{Hz}$.

3.3 Elasticity and fracturing of a clay mineral film confined to a drop surface

Ribbon structures can also be formed from clay mineral colloidal particles as shown in Fig. 9. Such clay mineral particles may adhere to one another most likely due to the presence of small amounts of water, forming a quasi-two-dimensional elastic ribbon. Figure 9 shows that when such an elastic ribbon is stretched it fractures in a direction depending on the external force. In this case the deformation of a drop is either prolate or oblate, and is induced by an AC E-field.

Conclusions

In the present study we investigate particle deposition dynamics on leaky-dielectric drops as a function of E-field strengths and types (alternating or direct). By increasing the applied E-field strength, the surface particle's packing arrangements become denser, resulting in a higher packing fraction. We relate the change of packing density to (i) the strengthened EHD flows inside and outside the drop working on the particles in the direction towards the equator, and (ii) the electro-deformation of the drop enabling the particles to re-locate in the direction along the ribbon. Further, we have demonstrated how the particle packing density can be further improved by applying an alternating E-field, inducing a shape (Oblate $\leftrightarrow$ Prolate) transition cycles which facilitates the jammed surface particles with space and time to find optimal arrangements.

We also find that the mechanical properties of the film is highly dependent on the particles: whereas monodisperse polystyrene beads form packed granular monolayers which "liquefies" upon shaking, we find that clay particles form cohesive quasi-two-dimensional elastic films that fracture upon shaking.

Our results can be useful in the fabrication of patchy particles [24] and for controlling the permeability and roughness of colloidal shells [25,26]. The results are expected to be relevant for understanding the mechanics and rheology of particle stabilized emulsions.

Z. Rozynek acknowledges financial support from the Foundation for Polish Science through Homing Plus programme.

References

1. A. van Blaaderen, M. Dijkstra, R. van Roij, A. Imhof, M. Kamp, B. Kwaadgras, T. Vissers, B. Liu, Eur. Phys. J. Special Topics **222**, 2895 (2013)
2. A.R.M. Verschueren, L.W.G. Stofmeel, P.J. Baesjou, M. van Delden, K.M.H. Lenssen, M. Mueller, G. Oversluizen, J.J. van Glabbeek, J.T.M. Osenga, R.M. Schuurbiers, J. Soc. Inform. Display **18**, 1 (2010)
3. D. Graham-Rowe, Nat. Photon. **1**, 248 (2007)
4. H. Lowen, Soft Matter **6**, 3133 (2010)
5. S. Nudurupati, M. Janjua, N. Aubry, P. Singh, Electrophoresis **29**(5), 1164 (2008)
6. S.R. Yeh, M. Seul, B.I. Shraiman, Nature **386**, 57 (1997)
7. P. Dommersnes, Z. Rozynek, A. Mikkelsen, R. Castberg, K. Kjerstad, K. Hersvik, J.O. Fossum, Nat. Commun. **4**, 2066 (2013)
8. W.D. Ristenpart, P. Jiang, M.A. Slowik, C. Punckt, D.A. Saville, I.A. Aksay, Langmuir **24**, 12172 (2008)
9. W.D. Ristenpart, I.A. Aksay, D.A. Saville, Phys. Rev. E **69**, 021405 (2004)
10. R.D. Deegan, O. Bakajin, T.F. Dupont, G. Huber, S.R. Nagel, T.A. Witten, Nature **389**, 827 (1997)
11. J.S. Jenkins, M.C. Flickinger, O.D. Velev, Materials **6**, 1803 (2013)
12. T.P. Bigioni, X.M. Lin, T.T. Nguyen, E.I. Corwin, T.A. Witten, H.M. Jaeger, Nat. Mater. **5**, 265 (2006)
13. P. Born, A. Munoz, C. Cavelius, T. Kraus, Langmuir **28**, 8300 (2012)
14. S. Watanabe, Y. Mino, Y. Ichikawa, M.T. Miyahara, Langmuir **28**, 12982 (2012)
15. R. Bhardwaj, X.H. Fang, P. Somasundaran, D. Attinger, Langmuir **26**, 7833 (2010)
16. G. Taylor, Proc. Royal Soc. A: Math. Phys. Eng. Sci. **291**, 159 (1966)
17. D.A. Saville, Annu. Rev. Fluid Mech. **29**, 27 (1997)
18. A.G. Marin, H. Gelderblom, D. Lohse, J.H. Snoeijer, Phys. Rev. Lett. **107** (2011)
19. K. Chen, J. Cole, C. Conger, J. Draskovic, M. Lohr, K. Klein, T. Scheidemantel, P. Schiffer, Nature **442**, 257 (2006)
20. G. Chen, P. Tan, S. Chen, J. Huang, W. Wen, L. Xu, Phys. Rev. Lett. **110**, 064502 (2013)
21. R. Aveyard, B.P. Binks, J.H. Clint, Adv. Coll. Interf. Sci. **100**, 503 (2003)
22. C.H. Chang, L.C. Wang [arXiv:1009.4322v1] (2010)
23. P.F. Salipante, P.M. Vlahovska, Phys. Fluids **22** (2010)
24. G.R. Yi, D.J. Pine, S. Sacanna, J. Phys. Condens. Mat. **25**, 193101 (2013)
25. A.D. Dinsmore, M.F. Hsu, M.G. Nikolaides, M. Marquez, A.R. Bausch, D.A. Weitz, Science **298**, 1006 (2002)
26. Z. Rozynek, A. Mikkelsen, P. Dommersnes, J.O. Fossum, Nat. Commun. **5**, 3945 (2014)